

## **The p7 protein of hepatitis C virus forms structurally plastic, minimalist ion channels**

Danielle E. Chandler<sup>1</sup>, François Penin<sup>2</sup>, Klaus Schulten<sup>3</sup>, Christophe Chipot<sup>4,\*</sup>

**1 Department of Physics and Beckman Institute, University of Illinois at Urbana-Champaign, Urbana, Illinois 61801**

**2 Bases Moléculaires et Structurales des Systèmes Infectieux, IBCP, Université Lyon 1, Univ Lyon, France; CNRS, UMR 5086 ; 7 passage du vercors, F-69367, Lyon, France**

**3 Department of Physics and Beckman Institute, University of Illinois at Urbana-Champaign, Urbana, Illinois 61801**

**4 Beckman Institute, University of Illinois at Urbana-Champaign Urbana, Illinois 61801**

**\* E-mail: Corresponding [chipot@ks.uiuc.edu](mailto:chipot@ks.uiuc.edu)**

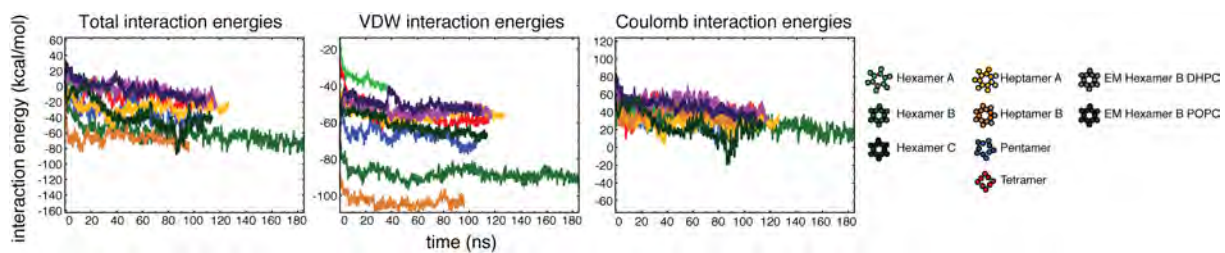


**Figure S1.** Interaction energies per subunit, averaged over the trajectory. Heptamer B and Hexamer B display lower total interaction energies. The differences in interaction energies between the models is clearly dominated by the van der Waals component.

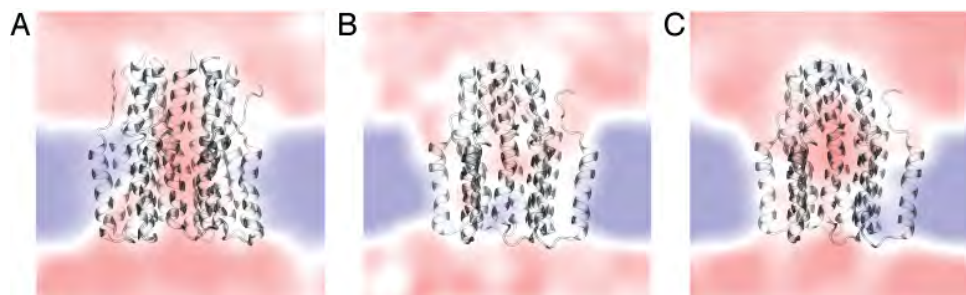


**Figure S2.** Electrostatic potential maps of (A) Heptamer B (B) Hexamer B before opening of pore (C) Hexamer B after opening of pore. The potential map of Hexamer B before the opening of the central pore shows a barrier between the interior of the pore and the solvent; the maps of Heptamer B and of Hexamer B after the opening of the pore show that the interior of the pore is accessible to solvent.

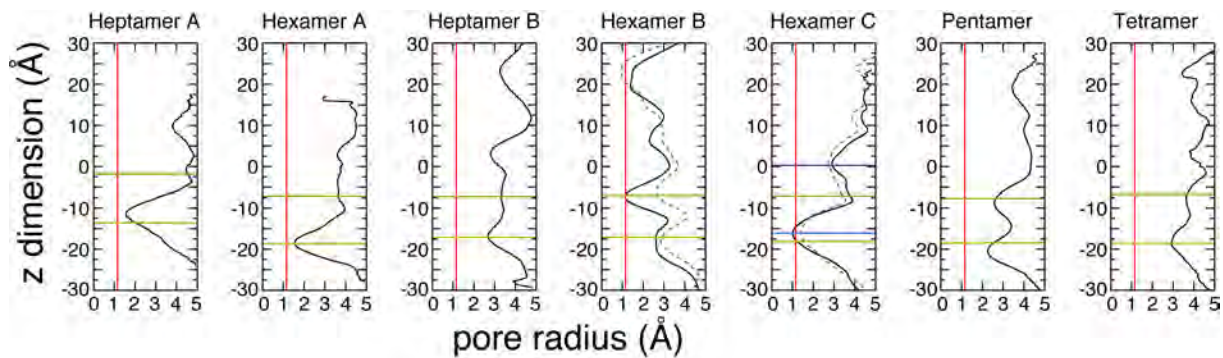


**Figure S3.** Radial profiles of each of the p7 models, calculated using HOLE. The green and yellow lines mark the positions of F25 and I32, respectively. In the Hexamer C plot, L20 and Y31 are also marked in purple and blue, respectively. In the Hexamer B and Hexamer C plots, the solid black profile represents the model before the opening of the pore, and the dashed gray profile represents the model afterwards.

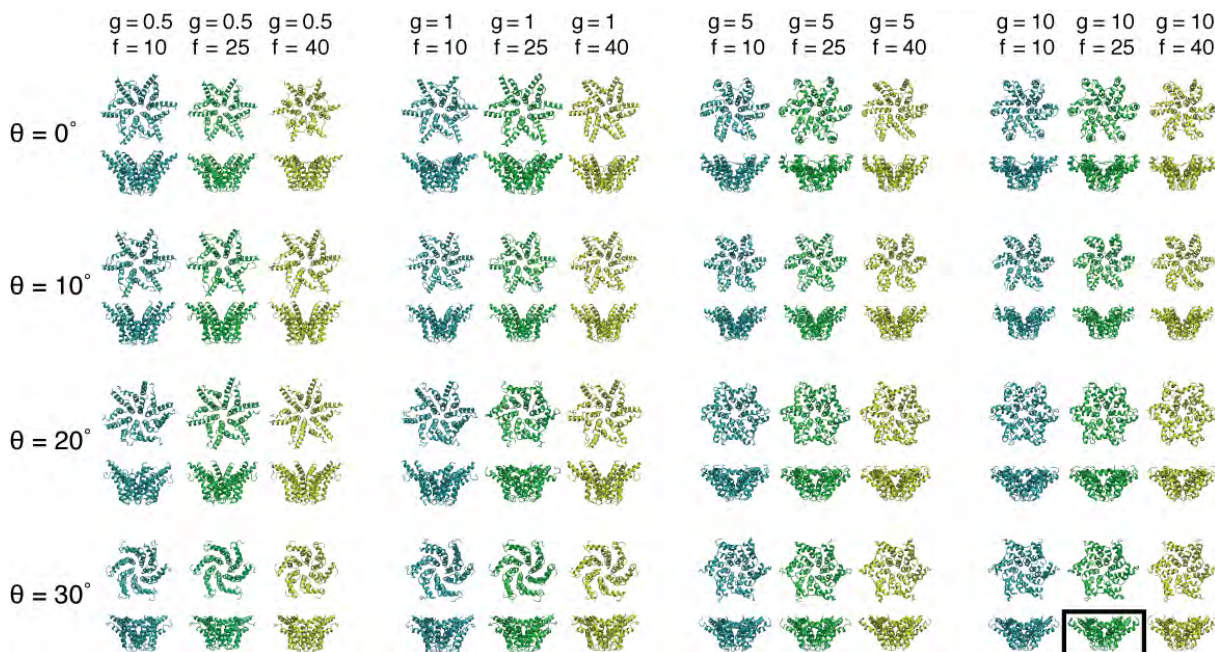


**Figure S4.** A variety of models obtained by driving the upright Hexamer B model into the 16 Å EM map, as determined by differences in starting conditions (in this case the rotation angle  $\theta$  about the central axis) and force constants ( $f$  and  $g$ ) used in the MDFF algorithm. It was clear that the model fit best into the map at  $\theta = 30^\circ$  but the authors were curious how the method would handle initial configurations that were rotated away from the correct orientation. The force constant  $f$  determines the strength of the symmetry constraints, while  $g$  determines the strength of the force driving the model into the EM map. The structures obtained from higher force constants tended to be more tilted than those obtained with lower force constants, even when MDFF was applied to the latter for considerably longer times. However, the larger force constants also tended to result in more helical distortion. We chose a model (highlighted above) which we felt represented a compromise between the conflicting goals of achieving a highly-bent corolla-like shape and not introducing excessive distortion.

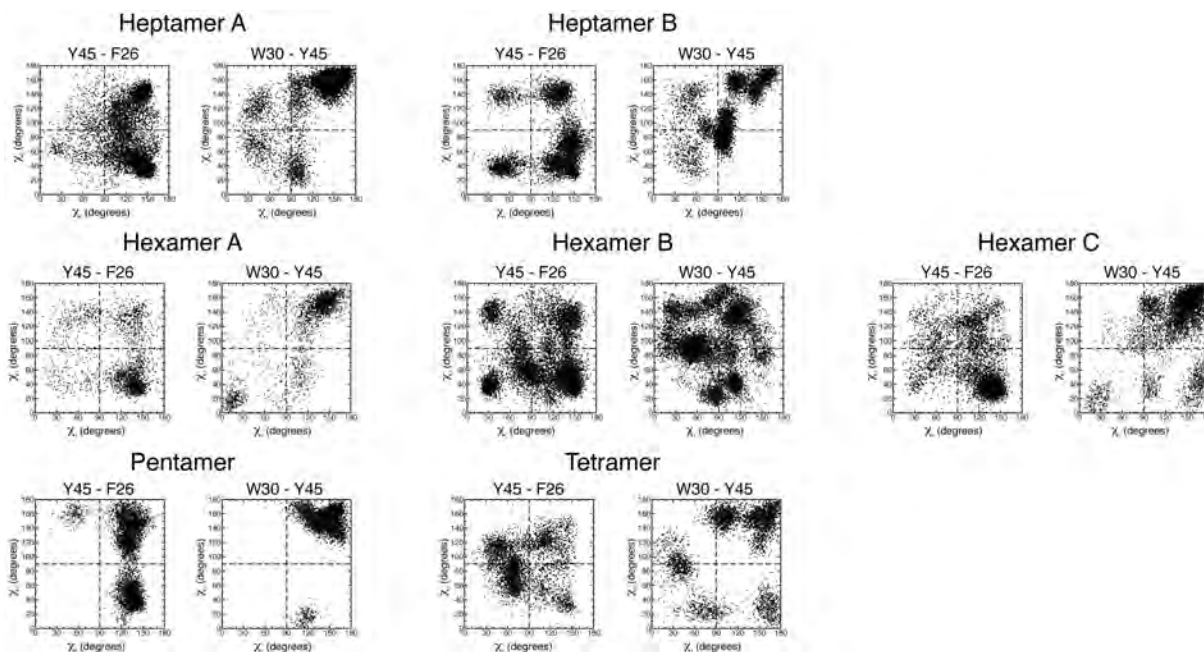


**Figure S5.** Angular distribution for the  $\pi$ - $\pi$  stacking interaction of residues F26 and Y45, and W30 and Y45, for each of the oligomeric p7 models.  $\chi_1$  and  $\chi_2$  are the angles formed by the normal  $n_1$  to the plane of the first aromatic ring and the vector  $u_{12}$  connecting the centroid of the two interacting aromatic rings, and by the normal  $n_2$  to the plane of the second aromatic ring and vector  $u_{12}$ . Combinations of  $\chi_1$  and  $\chi_2$  of approximately 0 or 180° correspond to  $\pi$ - $\pi$  stacked motifs of the aromatic side chains. The clustering of data points around the four corners of the graph show that the stacking interactions are roughly preserved in the oligomeric models.

Movie Description: **Movie1-MDFF.mpg**

Movie showing the upright Hexamer B model being driven into the EM density using the MDFF method.

Movie Description: **Movie2-HexamerB-trajectory.mpg**

Movie showing the simulation trajectory for the Hexamer B model; the pore opens during the simulation when the mutual interactions of the F25 side chains and I32 side chains are broken.

Movie Description: **Movie3-EMfitted-HexamerB-in-POPC.mpg**

Movie showing the trajectory for the EM-fitted Hexamer B model in a POPC bilayer; over the course of the trajectory, the helices begin to straighten as a result of hydrophobic mismatch.

Movie Description: **Movie4-K33Q-R35Q-HexamerB-conductance-simulation.mpg**

Movie showing the trajectory for an additional conductance simulation done with a K33Q-R35Q mutated Hexamer B model. The applied voltage was 1500 mV, and the system was simulated for 84 ns. Without the positively charged K33 and R35 blocking the entrance to the channel, potassium ions were able to enter and pass through the channel, and a cation selectivity, as seen in experiments, was observed. However, only a few ions passed through the channel over the course of the simulation, leading to a very small measured conductance value. This suggests that either our simulations are too short to reproduce the order of magnitude of the conductances measured in experiments, or that the ion parametrization is suboptimal.